Asymptotic Stress Field for the Blunt and Sharp Notches in Bi-Material Media Under Mode III Loading

ASME Journal of Applied Mechanics
Online journal at:
https://asmedigitalcollection.asme.org/appliedmechanics

Amir Mohammad Mirzaei[1]
Department of Structural,
Geotechnical and Building Engineering,
Politecnico di Torino,
Corso Duca degli Abruzzi 24,
Torino 10129, Italy
e-mail: amir.mirzaei@polito.it

Alberto Sapora
Department of Structural,
Geotechnical and Building Engineering,
Politecnico di Torino,
Corso Duca degli Abruzzi 24,
Torino 10129, Italy
e-mail: alberto.sapora@polito.it

Pietro Cornetti
Department of Structural,
Geotechnical and Building Engineering,
Politecnico di Torino,
Corso Duca degli Abruzzi 24,
Torino 10129, Italy
e-mail: pietro.cornetti@polito.it

Asymptotic Stress Field for the Blunt and Sharp Notches in Bi-Material Media Under Mode III Loading

This study introduces a novel approach to analyze the stress and displacement fields around blunt notches in bi-material media, focusing on mode III loading conditions. The eigenfunction expansion method is used to derive a simplified yet accurate solution, satisfying the boundary conditions for bi-material blunt V-notches. The robustness of the proposed asymptotic solution is validated through several finite element analyses, encompassing a range of notched geometries such as blunt V-notches, VO-notches, and circular holes. Notably, it is demonstrated that when the notch tip radius approaches zero, the solution coincides with the existing sharp V-notch model. [DOI: 10.1115/1.4064323]

Keywords: bi-material media, asymptotic expansion, interfacial notches, torsion, out-of-plane loading, elasticity, stress analysis

1 Introduction

Understanding the stress distribution around V-notches in dissimilar material interfaces is crucial for various engineering applications, including (a) designing and optimizing mechanical joints and interfaces, (b) assessing and preventing failure in structures subject to heavy loads or repeated stress cycles, (c) developing new materials and composite structures, (d) improving manufacturing processes, and (e) enhancing safety in various industries such as aerospace. Despite the availability of advanced numerical tools capable of handling such scenarios, the analysis of large structures often becomes impractical due to the requirement of high mesh resolutions. This becomes especially challenging in Mode III, where 3D simulations are required. In the following, a review of studies related to this investigation is presented.

While extensive research has been conducted on mode I and mode II, with notable contributions from Williams [1] and Bogy [2,3], the exploration of mode III fracture mechanics, characterized by out-of-plane shear stresses, has been relatively limited in the literature. This is primarily due to the challenges in experimental validation of mode III phenomena, higher computational demands, and possible overlaps and interactions between mode III and other modes of loading. Nevertheless, pioneering works by Ma and Hour [4] have provided analytical solutions for isotropic and anisotropic bi-material V-notches under antiplane deformation. Champion et al. [5] examined the stress singularity at the crack tip in different power-law materials under mode III loading, revealing that stress singularities are identical in each material, equivalent to a crack in a homogeneous material with the maximum hardening exponent. Moreover, they found that all the crack-tip energy is concentrated in the material with the largest hardening exponent. Karganovin and colleagues [6] developed a solution for an isotropic finite wedge, while Shahani [7] extended this solution to an anisotropic monolithic wedge and later derived a solution for an isotropic bi-material wedge [8]. Using matched asymptotic expansions, Leguillon and Abdelmoula [9] obtained a solution for two different elastic substrates connected by a thin adhesive layer with a crack under antiplane loading. Their research defines two types of mode III stress intensity factors based on crack location and considers interface conditions and material properties. Tuyet et al. [10] explored the impact of small defects, such as cavities or cracks, on a linear-elastic material using a matched asymptotic expansion method. A detailed analysis in an antiplane setting, particularly for a small crack, was conducted, followed by a comparative study with classical finite element method results. Mishuris et al. [11] analyzed the stress and displacement fields near a crack tip moving along a bi-material interface with a thin separating layer. They also derived asymptotic formulae for displacement and stress intensity factors under out-of-plane loading, validating the results through numerical analyses.

Paggi and Carpinteri [12] presented a noteworthy contribution by providing a formal solution for an isotropic multi-material wedge subjected to mode III displacement. They showcased that the problem solution does not necessarily rely on the Mellin transform but can be achieved through the eigenfunction expansion method. Similarly, Savruk and Kazberuk [13] and Frishter [14] derived a near-vertex stress field solution for a symmetric isotropic monolithic V-notch under remote mode I, mode II, and mode III loading.

To address the anisotropic bi-material wedge problem, Beom and Jang [15] utilized a complex function to represent the homogeneous wedge. By applying a linear transformation method to convert the anisotropic bi-material wedge into an isotropic bi-material wedge,

[1]Corresponding author.

Manuscript received September 14, 2023; final manuscript received December 12, 2023; published online January 29, 2024. Assoc. Editor: Pradeep Sharma.

they transferred the boundary conditions and continuity equations into complex space, deriving a characteristic equation for the singularity. Eder and Sarhadi [16] introduced a semi-analytical solution to correct the numerical near-singularity stress field near reentrant corners in bi-material interface V-notches under mode III loading. This method proves beneficial for fatigue lifetime analysis of large structures as it reduces the computational costs associated with high-resolution discretization in large-scale numerical engineering models. In a recent study, Jiménez-Alfaro and Mantič [17] investigated the mode III crack-tip solution for a semi-infinite crack located in a straight spring interface within an infinite linear elastic isotropic solid. They expressed the crack-tip solution as a double asymptotic series consisting of main and associated shadow terms, which includes logarithmic terms. The effect of higher order terms for sharp V-notches in bi-material media was demonstrated by Bahrami et al. [18]. They employed the overdeterministic technique to determine the coefficients of higher order terms, highlighting their significance in calculations.

Considering samples weakened by blunt V-notches under mixed mode I/II loading, Mirzaei et al. [19] developed a new asymptotic stress field solution using Kolosov–Muskhelishvili's approach. Their solution demonstrates higher accuracy for blunt V-notches compared to previous methods and its applicability to various blunt notch geometries. Furthermore, Mirzaei et al. [20] extended the same approach to bi-material blunt notches, presenting the first stress field solution for this type of notch under mixed mode loading. This paper focuses on developing a novel approach to obtain, for the first time, the stress and displacement fields around blunt notches in bi-material media under mode III loading. The paper is structured as follows: Sec. 2 presents a detailed statement of the problem and the development of the solution. In Sec. 3, a brief analysis is conducted to determine the stress intensity factor and higher order terms of the solution. Validation of the proposed asymptotic solution through comparison with finite element analysis is presented in Sec. 4. The results demonstrate that the model is not only applicable to blunt V-notches but also provides high accuracy for other types of notches, such as VO-notches and holes.

2 Statement of Problem

The present section addresses the mathematical modeling of the problem. First, the fundamental equations are introduced, and subsequently, by satisfying the boundary conditions, the asymptotic displacement and stress fields around a blunt V-notch in a bi-material medium are determined. It is assumed that both bodies are homogeneous, and isotropic, following linear-elastic behavior. Considering the fundamental equations of elasticity for out-of-plane loading and neglecting both inertia and body force, the equilibrium condition for a thin plate can be expressed in terms of the displacement component $w(r, \theta)$. The resulting equation, given by the two-dimensional Laplacian operator, is $\nabla^2 w(r, \theta) = 0$. The model assumes small deflections and is applicable in scenarios where the thickness of the plate is smaller than its other dimensions. By employing the eigenfunction expansion method and assuming $w(r, \theta) = r^{\lambda_n} f_n(\theta, \lambda_n)$, the solution for the Laplace's equation can be achieved:

$$w(r, \theta) = \sum_{n=1}^{\infty} r^{\lambda_n} (A_n \cos[\lambda_n \theta] + B_n \sin[\lambda_n \theta]) \tag{1}$$

where λ is called the eigenvalue of the problem and is greater than zero.

By taking inspiration from Eq. (1), in order to satisfy additional boundary conditions associated with the tip of the notch, we assume $w(r, \theta) = r^{\lambda_n} f_n(\theta, \lambda_n) + r^{-\lambda_n} g_n(\theta, \lambda_n)$. Substituting this expression into Laplace's equation yields the governing equation for the problem:

$$w(r, \theta) = \frac{1}{\mu} \sum_{n=1}^{\infty} r^{\lambda_n} (A_n \cos[\lambda_n \theta] + B_n \sin[\lambda_n \theta]) + r^{-\lambda_n} (C_n \cos[\lambda_n \theta] + D_n \sin[\lambda_n \theta]) \tag{2}$$

where μ is the shear modulus. It is worth noting that Eq. (2) still fulfills the equilibrium equation. The selection of the second term in Eq. (2) is designed strategically, such that it exerts a significant influence in the vicinity of the tip, while gradually diminishing as the distance from the notch tip increases. Then, considering Hook's law, shear stress components are as follows:

$$\sigma_{zr}(r, \theta) = \mu \frac{\partial w(r, \theta)}{\partial r} \tag{3a}$$

$$\sigma_{z\theta}(r, \theta) = \frac{\mu}{r} \frac{\partial w(r, \theta)}{\partial \theta} \tag{3b}$$

2.1 Boundary Conditions. In order to determine the eight free parameters, A_n^k, B_n^k, C_n^k, and D_n^k ($k = 1, 2$), boundary conditions need to be applied. In this study, the superscripts 1 and 2 are representative of materials 1 and 2. In brief, according to Fig. 1, these boundary conditions encompass the continuity of stress and displacement components along the interface, as well as traction-free conditions on the notch border, which includes the notch flanks and notch tip.

Continuity of the stress and displacement components along the interface, $\theta = 0$, can be written as follows:

$$w^1 = w^2 \tag{4a}$$

$$\sigma_{z\theta}^1 = \sigma_{z\theta}^2 \tag{4b}$$

By satisfying the traction-free condition on the notch flanks, we have:

$$\sigma_{z\theta}^1|_{\theta=\gamma_1-\arcsin(\frac{\rho}{r})} = \sigma_{z\theta}^2|_{\theta=-(\gamma_2-\arcsin(\frac{\rho}{r}))} = 0, \quad (r > \rho) \tag{5}$$

To simplify the mathematical complexity and obtain the eigenvalues, Eq. (5) can be satisfied at $r \to \infty$, which corresponds to far distances from the notch tip. Consequently, $\arcsin(\rho/r) \to 0$ and $r^{-\lambda} \to 0$ (since $\lambda > 0$, see Eq. (2)). The approach was previously used in several investigations [19, 20]. Note that this simplification results in an approximate solution, not an exact one.

To satisfy the boundary conditions at the notch tip, the traction-free condition must be imposed, which dictates that:

$$\sigma_{zr}^1|_{r=\rho} = 0 \tag{6a}$$

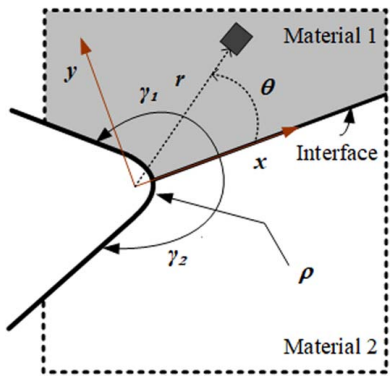

Fig. 1 A schematic view of the geometrical parameters related to a blunt V-notch in a bi-material medium along with polar and Cartesian coordinate systems. Note that the origin of both coordinate systems is at the center of curvature of the notch tip.

$$\sigma^2_{zr}|_{r=\rho} = 0 \tag{6b}$$

It is important to recognize that in this problem, there are eight free parameters, denoted as $A^k_n, \ldots, D^k_n (k = 1, 2)$, while there are only six boundary conditions. The way to reconcile this disparity will be elucidated by Eq. (7).

Equations (6*a*) and (6*b*), respectively, result in:

$$(-D^1_n + B^1_n \rho^{2\lambda_n}) \cos[\theta\lambda_n] - (C^1_n - A^1_n \rho^{2\lambda_n}) \sin[\theta\lambda_n] = 0 \tag{7a}$$

$$(-D^2_n + B^2_n \rho^{2\lambda_n}) \cos[\theta\lambda_n] - (C^2_n - A^2_n \rho^{2\lambda_n}) \sin[\theta\lambda_n] = 0 \tag{7b}$$

Note that Eqs. (7*a*) and (7*b*) must be satisfied for any θ and λ. As $\sin[\theta\lambda_n]$ and $\cos[\theta\lambda_n]$ are linearly independent over their period, the only way for their linear combination to be exactly zero is for both terms to be zero. In this case, two equations can be extracted from each, resulting in the four following simple equations:

$$D^k_n = B^k_n \rho^{2\lambda_n},\ C^k_n = A^k_n \rho^{2\lambda_n}, \quad k = 1, 2 \tag{8}$$

Considering Eqs. (4) and (5), and by employing the eigenvalue method [1–3]—which involves using $m-1$ equations from a system of m linear equations to identify relationships between coefficients—relations between $A_n{}^1$, $B_n{}^1$, $B_n{}^2$ based on $A_n{}^2$ can be determined as follows:

$$A^1_n = A^2_n \tag{9a}$$

$$B^1_n = \cot[(\pi - \alpha_1)\lambda_n] A^2_n \tag{9b}$$

$$B^2_n = -\cot[(\pi - \alpha_2)\lambda_n] A^2_n \tag{9c}$$

where $\alpha_1 = \pi - \gamma_1$ and $\alpha_2 = \pi - \gamma_2$ represent the notch opening angles of materials 1 and 2, respectively, with respect to the interface.

To avoid trivial solutions for the system of equations presented by Eqs. (4) and (5), the determinant of the system (containing all four equations) must be set equal to zero. This condition leads to the following equation:

$$\frac{\mu_2}{\mu_1} \cos[(\pi - \alpha_1)\lambda_n] \sin[(\pi - \alpha_2)\lambda_n] + \cos[(\pi - \alpha_2)\lambda_n] \sin[(\pi - \alpha_1)\lambda_n] = 0 \tag{10}$$

Equation (10) provides eigenvalues of the problem, λ_n, and it has infinite solutions. Given that Eqs. (4) and (5) are valid for sharp V-notches, eigenvalues are identical to those of sharp V-notches.

Finally, by replacing all the free parameters based on one free parameter, $A_n{}^2$, the stress components in a polar coordinate system located at the notch tip center of curvature are:

$$\sigma^1_{zr} = \sum_{n=1}^{\infty} A^2_n r^{\lambda_n - 1} \left(1 - \left(\frac{\rho}{r}\right)^{2\lambda_j}\right) (\cos[\theta\lambda_n] \cot[(\pi - \alpha_1)\lambda_n] + \sin[\theta\lambda_n]) \lambda_n \tag{11a}$$

$$\sigma^2_{zr} = \sum_{n=1}^{\infty} A^2_n r^{\lambda_n - 1} \left(1 - \left(\frac{\rho}{r}\right)^{2\lambda_j}\right) (-\cos[\theta\lambda_n] \cot[(\pi - \alpha_2)\lambda_n] + \sin[\theta\lambda_n]) \lambda_n \tag{11b}$$

$$\sigma^1_{z\theta} = \sum_{n=1}^{\infty} A^2_n r^{\lambda_n - 1} \left(1 + \left(\frac{\rho}{r}\right)^{2\lambda_j}\right) (\cos[\theta\lambda_n] - \cot[(\pi - \alpha_1)\lambda_n] \sin[\theta\lambda_n]) \lambda_n \tag{11c}$$

$$\sigma^2_{z\theta} = \sum_{n=1}^{\infty} A^2_n r^{\lambda_n - 1} \left(1 + \left(\frac{\rho}{r}\right)^{2\lambda_j}\right) (\cos[\theta\lambda_n] + \cot[(\pi - \alpha_2)\lambda_n] \sin[\theta\lambda_n]) \lambda_n \tag{11d}$$

The displacement components are as follows:

$$w^1 = \sum_{n=1}^{\infty} A^2_n \frac{r^{\lambda_n}}{\mu_1} \left(1 + \left(\frac{\rho}{r}\right)^{2\lambda_j}\right) (\cos[\theta\lambda_n] \cot[(\pi - \alpha_1)\lambda_n] + \sin[\theta\lambda_n]) \tag{12a}$$

$$w^2 = \sum_{n=1}^{\infty} A^2_n \frac{r^{\lambda_n}}{\mu_2} \left(1 + \left(\frac{\rho}{r}\right)^{2\lambda_j}\right) (-\cos[\theta\lambda_n] \cot[(\pi - \alpha_2)\lambda_n] + \sin[\theta\lambda_n]) \tag{12b}$$

In Eqs. (11) and (12), the effect of the notch tip radius on stress and displacement fields is clear.

3 Stress Intensity Factor and Higher Order Terms

As mentioned earlier, Eq. (10) has infinite solutions, and the eigenvalues and eigenfunctions of the problem are defined based on α_1 and α_2 as well as the ratio between μ_1 and μ_2. Note that differently from the in-plane problem, the eigenvalues of mode III loading are always real numbers. In order to simplify the calculations and consider only the first term in analyses which has the highest impact in calculations, the first free parameter, A^2_1, can be determined by fitting either stress or displacement component obtained from finite element analysis or experimental techniques such as photoelasticity or digital image correlation (DIC).

By following the definition of the stress intensity factor for interfacial sharp notches and cracks, we can obtain it for the proposed solution as follows [21]:

$$K_{III} = \lim_{r \to 0} \frac{\sigma_{z\theta}|_{\theta=0}}{(2\pi r)^{\lambda_1 - 1}} \tag{13}$$

According to Eq. (13) the relation between K_{III} and A^2_1 can be expressed as follows:

$$A^2_1 = \frac{(2\pi)^{\lambda_1 - 1}}{\lambda_1 \lim_{r \to \rho} \left[1 + \left(\frac{\rho}{r}\right)^{2\lambda_1}\right]} K_{III} \tag{14}$$

Considering the case of bi-material blunt notches in mixed modes I/II where higher order terms play an important role, we employ both the first and the second terms of the truncated series. Following Refs. [22,23], the determination of the free coefficients by considering the higher order terms can be achieved through a fitting procedure, employing either a deterministic or an overdeterministic system of equations. For the sake of brevity, the details of obtaining the coefficients for higher order terms (specifically $n = 2$ in this paper) are not provided in this paper. Interested readers are referred to Refs. [22,23] for further information.

4 Numerical Examples

The stress and displacement fields around blunt V-notches were derived in an asymptotic form, incorporating one free parameter for each term. In this part, it is shown that the proposed asymptotic stress field is capable of determining the stress distribution around some different blunt notches, with good accuracy. To verify this claim and assess the precision of Eq. (11), various types of notches with arbitrary geometries are considered and finite element analysis (FEA) is employed to compare the results obtained from both approaches.

For each sample, a 3D surface plot is constructed, illustrating the stress field around the notch tip. This plot incorporates the first two terms of the truncated series for both stress components and compares these findings with results obtained via FEA. Additionally, to more precisely show the accuracy of the proposed stress field and to illustrate the calculations using not only the first two terms but also the first term alone, the normalized stress component

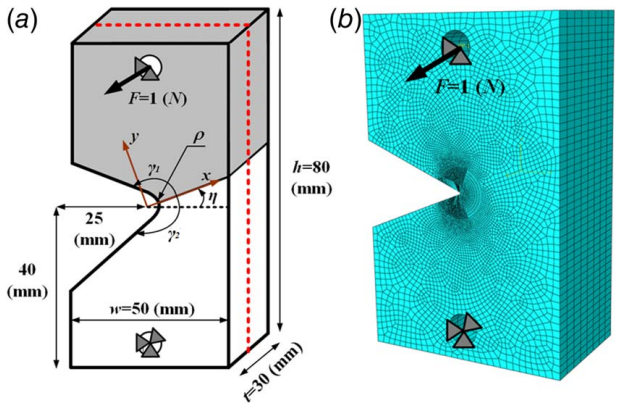

Fig. 2 The geometry, dimensions, and loading condition of the samples which are used to simulate the specimens in finite element analysis

along the circular path of $r/\rho = 2$ is provided, except for the sharp notch case where $r = 0.3$ mm.

For simplicity in simulating and meshing the samples, a specimen resembling a single edge notch tension (SENT) test is chosen. Mode III is introduced by applying an arbitrary out-of-plane load with a magnitude of $F = 1$ N. A schematic view of the loading condition is depicted in Fig. 2(*a*), while Fig. 2(*b*) illustrates the simulated sample of the blunt V-notch case within FEA.

It should be noted that the height, width, and thickness of specimens, as well as the applied load, and location of the notch tip center of curvature, remain constant throughout all simulations. To present the results, data provided by the midplane of each sample, indicated by the red dashed line in Fig. 2(*a*), are considered. Furthermore, an arbitrary combination of material properties is considered for the upper and lower bodies: for Material 1 (upper body), an elastic modulus of $E = 1$ MPa and Poisson's ratio $\nu = 0.25$ are chosen, while for Material 2 (bottom body), we employ the elastic modulus of $E = 5$ MPa and Poisson's ratio $\nu = 0.35$. These intentionally contrasting material properties are chosen to emphasize the accuracy of the proposed stress field and illustrate the influence of higher order terms. It should be noted that all the components are normalized by the maximum out-of-plane hoop stress at the notch tip, denoted as $\sigma_{z\theta}(0, \theta) = \sigma_{z\theta,tip}$.

In Figs. 3–7, results are presented: parts (*a*) and (*c*) depict a surface plot of the stress component, while parts (*b*) and (*d*) illustrate the corresponding stress component of parts (*a*) and (*c*), respectively, on a circular path $r/\rho = 2$ traversing from one side of the notch flank to another one. To help visualize the notch position in parts (*a*) and (*c*), it should be noted that the line $y = 0$ represents the interface between the two bodies. Also, a schematic view of each notch geometry is plotted in the part (*a*). It is worth mentioning that the notch geometries in the numerical examples are determined based on the notch opening angle (α_m), which is defined as $\alpha_k = \pi - \gamma_k$, $k = 1,2$. In the following, we present the results of the model validation for various notch geometries.

4.1 Sharp V-Notch. The proposed stress field can be applied to sharp V-notches by setting $\rho = 0$ in Eq. (11). Due to the selection of suitable eigenfunctions and boundary conditions, this solution is consistent with the solution provided by Qian and Hasebe [24] for bi-material sharp V-notches and cracks. This claim is substantiated by an illustrative example where the notch geometry parameters are $\alpha_1 = \pi/3$, $\alpha_2 = \pi/12$, $\eta = \pi/6$. Figure 3 provides the corresponding results for this particular notch geometry.

4.2 VO- and Key-Hole Notch. One practical method for reducing the high stresses induced by sharp notches and cracks is the introduction of stop-holes at their tips. This method modifies the sharp V-notch and crack geometries, turning them into VO- and key-hole notches. To evaluate the applicability of the proposed stress field for this category of notches, a specimen with a specific notch geometry $\alpha_1 = \pi/8$, $\alpha_2 = \pi/8$, $\eta = 0$, $\rho = 0.25$ (mm) is

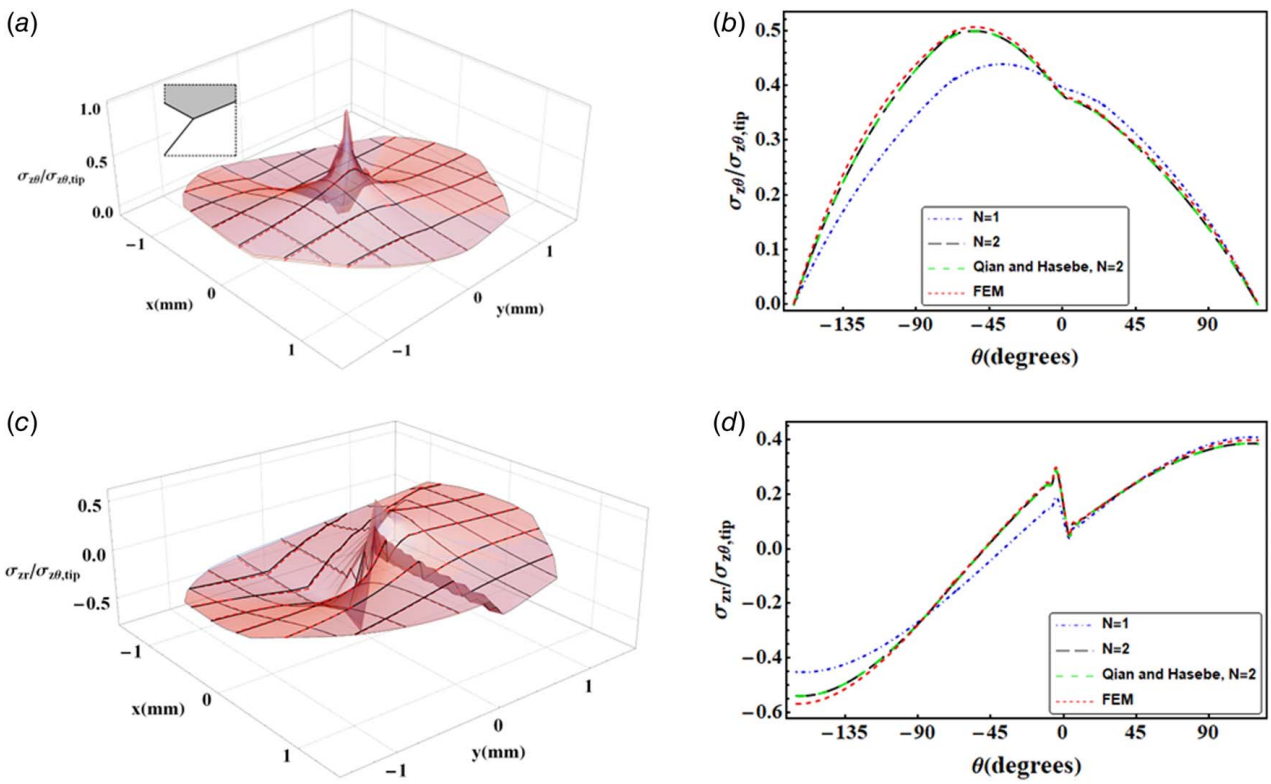

Fig. 3 Normalized stress field results obtained using the first two terms of Eq. (11) compared with FEA: (*a*) surface plot of $\sigma_{z\theta}$, (*b*) $\sigma_{z\theta}$ on a circular path $r = 0.3$ mm, (c) surface plot of σ_{zr}, (*d*) σ_{zr} on a circular path $r = 0.3$ mm

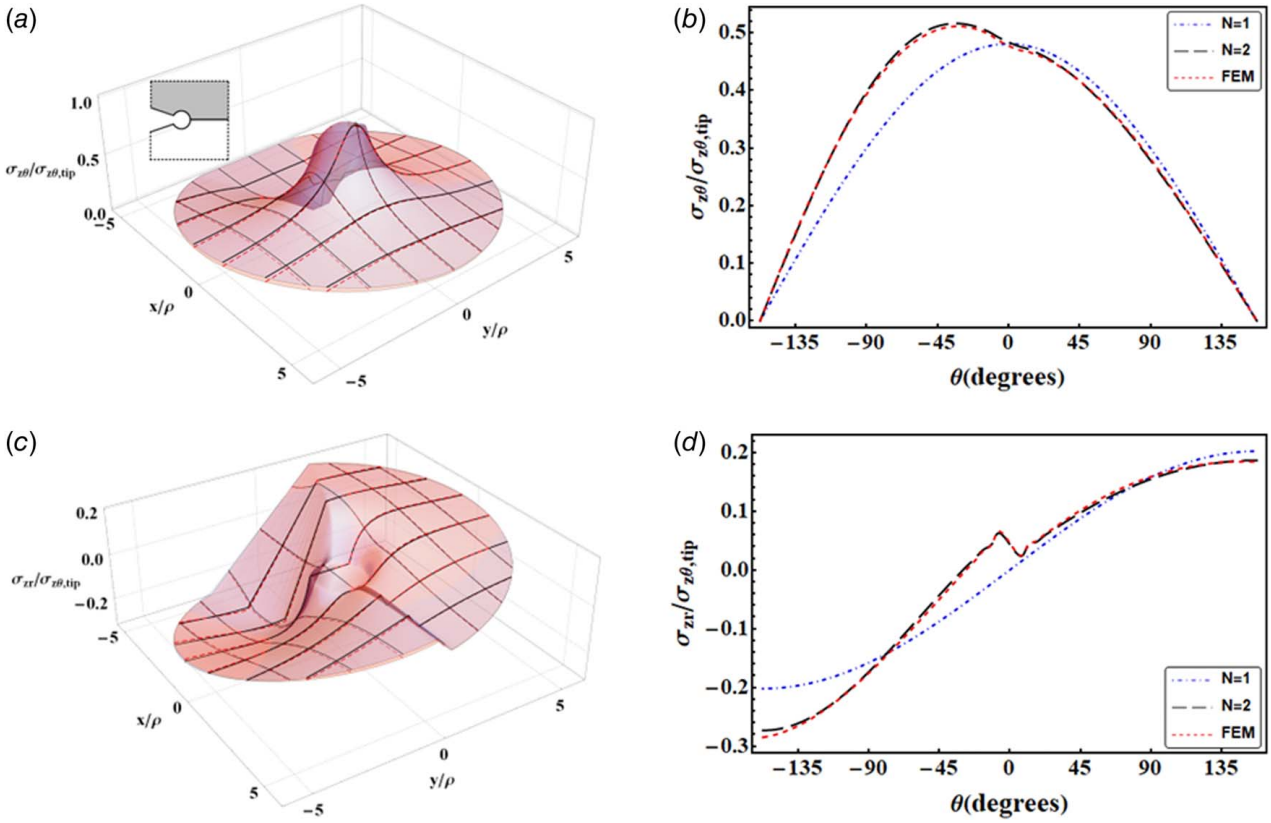

Fig. 4 Normalized stress field results obtained using the first two terms of Eq. (11) compared with FEA: (*a*) surface plot of $\sigma_{z\theta}$, (*b*) $\sigma_{z\theta}$ on a circular path $r/\rho = 2$, (*c*) surface plot of σ_{zr}, and (*d*) σ_{zr} on a circular path $r/\rho = 2$

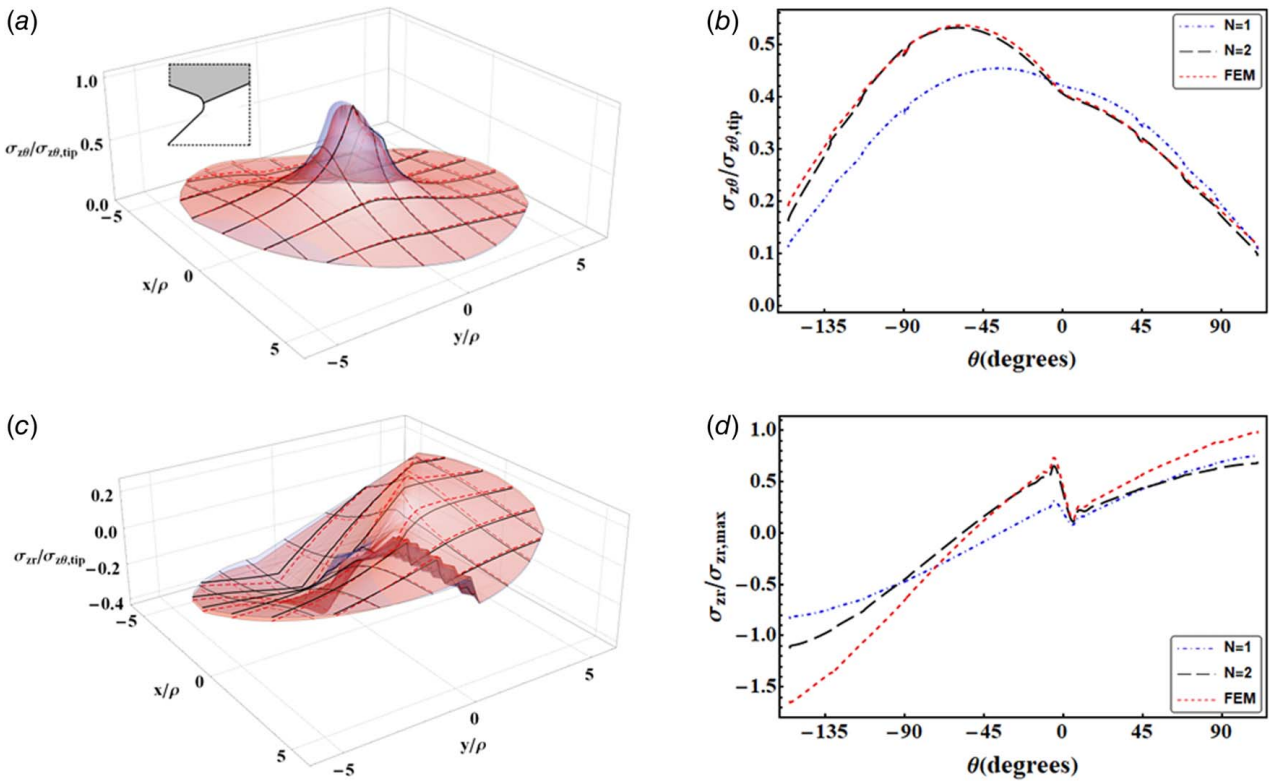

Fig. 5 Normalized stress field results obtained using the first two terms of Eq. (11) compared with FEA: (*a*) surface plot of $\sigma_{z\theta}$, (*b*) $\sigma_{z\theta}$ on a circular path $r/\rho = 2$, (*c*) surface plot of σ_{zr}, and (*d*) σ_{zr} on a circular path $r/\rho = 2$

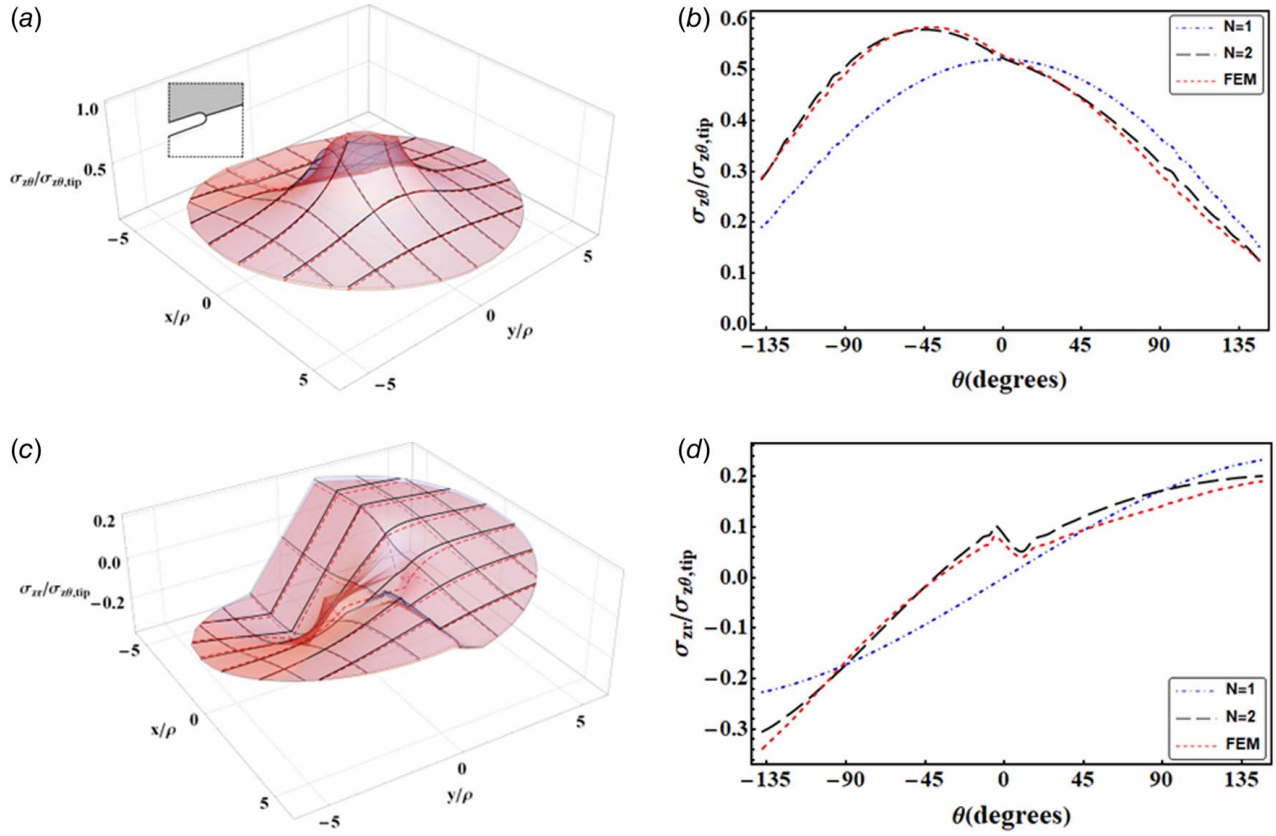

Fig. 6 Normalized stress field results obtained using the first two terms of Eq. (11) compared with FEA: (*a*) surface plot of $\sigma_{z\theta}$, (*b*) $\sigma_{z\theta}$ on a circular path $r/\rho = 2$, (c) surface plot of σ_{zr}, and (*d*) σ_{zr} on a circular path $r/\rho = 2$

examined. Figure 4 presents the results of this simulation, highlighting the efficacy of the proposed stress field in capturing the stress distribution for these types of blunt notches.

4.3 Blunt V-Notch. To evaluate the accuracy of the proposed solution in predicting the stress distribution around blunt V-notches, an arbitrary notch geometry is examined. In this example, the geometric parameters are set as $\alpha_1 = \pi/4$, $\alpha_2 = 0$, $\eta = \pi/8$, $\rho = 0.3$ (mm). The resulting stress components corresponding to this problem are illustrated in Fig. 5.

4.4 U-Notch. By reducing the notch opening angle of blunt V-notches to zero, while preserving the rounded tip, a well-known category of notches known as U-notches is obtained. As U-notches are widely used in various applications, it is essential to evaluate the applicability of the proposed solution. To this end, a notch with the following geometry parameters is considered: $\alpha_1 = 0$, $\alpha_2 = 0$, $\eta = \pi/6$, $\rho = 0.2$ (mm). Figure 6 showcases a comparison between the stress field ahead of the U-notch using the proposed solution and the results obtained from FEA.

4.5 Circular Hole. Given the significant influence of circular holes on the load-bearing capacity of structures, particularly in the context of drilling and rivet holes, it is crucial to investigate the applicability of the asymptotic stress field in determining the stress distribution around such holes in bi-material media. In Fig. 7, a specimen similar to Fig. 2(*b*), featuring a centrally located drilling hole, is analyzed to assess the proposed stress field. The geometric parameters for this case are set as follows: $\alpha_1 = \pi/2$, $\alpha_2 = \pi/2$, $\eta = 0$, $\rho = 0.2$ (mm).

This section provided insights into the effectiveness of the asymptotic stress field in accurately characterizing the stress distribution surrounding various blunt notches in different bi-material configurations. The impact of higher order terms, as indicated by Ref. [18], may vary depending on the notch geometry and the differences in material properties between the bodies. Upon analyzing several notch geometries, a noticeable influence of the second term was observed, even at close distances to the notch tip. However, a perfect match between the analytical and numerical solutions was not achieved. For this reason, it is important to note that the precision of Qian and Hasebe's solution [24], when considering the first two terms, was also not particularly perfect for sharp V-notches (Example 4.1). This discrepancy may be attributed to the complexities involved in modeling a pure mode III problem in FEA or the simplification of the governing equations. On the other hand, the proposed solution for blunt notches approximates the description of the notch geometry (Eq. (5)). It is worth mentioning that any asymptotic stress field has limited validity; i.e., it holds approximate values of the stress field in a finite region surrounding the notch. The extent of this region may differ from case to case; it is difficult to determine the effect of geometry and loading onto the region of validity of our analytical asymptotic solution. For instance, in the simplest case of a sharp notch in an isotropic monomaterial, the accuracy of the analytical solution may decrease when the notch depth becomes significant relative to the component's dimensions (due to boundary effects), or when the sample geometry is complex (e.g., a Brazilian Disk with a rhombus hole, compared to a Compact Tension specimen) [22,23]. In the case of blunt notches, the radius at the notch tip plays a predominant role and should be kept relatively small [19]. The complexity increases for bi-material notches due to the elastic mismatch between the materials [20]. In these situations, the accuracy of an asymptotic solution may diminish, and including additional higher-order terms could be quite beneficial. Nevertheless, the proposed asymptotic solution demonstrates an accurate representation of the stress field around different notch geometries with arbitrary material properties.

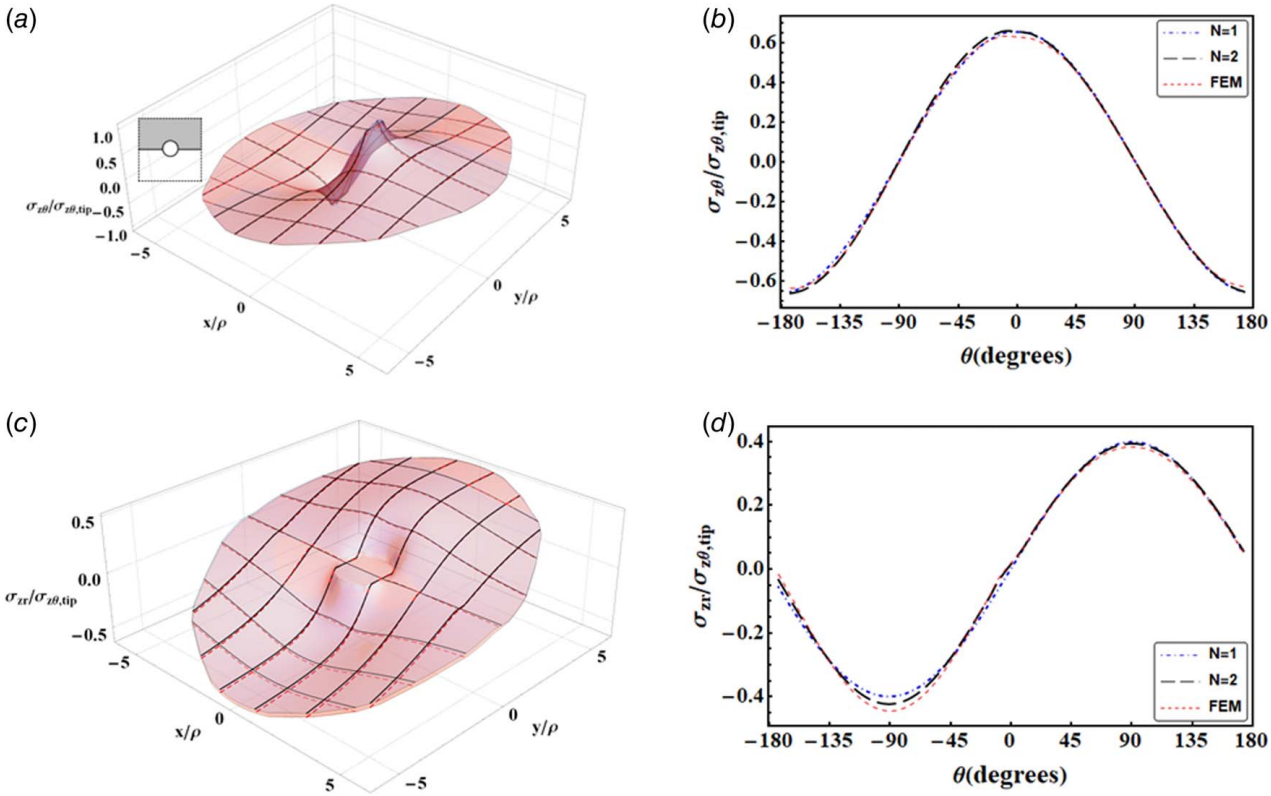

Fig. 7 Normalized stress field results obtained using the first two terms of Eq. (11) compared with FEA: (*a*) surface plot of $\sigma_{z\theta}$, (*b*) $\sigma_{z\theta}$ on a circular path $r/\rho = 2$, (c) surface plot of σ_{zr}, and (*d*) σ_{zr} on a circular path $r/\rho = 2$

The findings presented in this study may have significant implications for the field of fracture mechanics and provide valuable insights into the mechanical behavior of bi-material blunt notches under mode III loading. Our rigorous methodology along with its accurate results offers researchers and engineers a powerful tool for predicting stress distribution and displacement fields in complex fracture scenarios.

5 Conclusion

In this study, the eigenfunction expansion method was used to derive the stress and displacement components in the vicinity of a bi-material blunt V-notch under mode III loading. By satisfying the boundary conditions, the free parameters of the stress and displacement components were obtained based on a single free parameter for each term. No conformal mapping was used to describe the notch geometry, resulting in a solution that is independent of the accuracy of conformal mapping. By using appropriate eigenfunction and boundary conditions, the eigenvalues were shown to be equivalent to those of sharp V-notches, making the solution easier to use in calculating the stress field. To assess the accuracy and reliability of the approach, a comprehensive comparative analysis was conducted. Through the evaluations, remarkable agreement was demonstrated between the analytical stress field results obtained from the proposed method and the results obtained through finite element analysis. This agreement was observed across various cases of blunt notches, encompassing the geometries of VO- and key-hole-notches, V- and U-notches, and circular holes in bi-material media.

Acknowledgment

The authors acknowledge the funding from the European Union's Horizon 2020 research and innovation program under the Marie Skłodowska-Curie Grant Agreement No 861061—NEWFRAC Project.

Conflict of Interest

There are no conflicts of interest.

Data Availability Statement

The datasets generated and supporting the findings of this article are obtainable from the corresponding author upon reasonable request.

References

[1] Williams, M. L., 1952, "Stress Singularities Resulting From Various Boundary Conditions in Angular Corners of Plates in Extension," ASME J. Appl. Mech., **19**(4), pp. 526–528.
[2] Bogy, D. B., 1971, "On the Plane Elastostatic Problem of a Loaded Crack Terminating at a Material Interface," ASME J. Appl. Mech., **38**(4), pp. 911–918.
[3] Bogy, D. B., 1971, "Two Edge-Bonded Elastic Wedges of Different Materials and Wedge Angles Under Surface Tractions," ASME J. Appl. Mech., **38**(2), pp. 377–386.
[4] Ma, C.-C., and Hour, B.-L., 1989, "Analysis of Dissimilar Anisotropic Wedges Subjected to Antiplane Shear Deformation," Int. J. Solids Struct., **25**(11), pp. 1295–1309.
[5] Champion, C. R., Atkinson, C., and Bilby, B. A., 1990, "A Mode III Crack at the Interface Between Two Nonlinear Materials," Proc. R. Soc. A, **429**(1876), pp. 247–257.
[6] Kargarnovin, M. H., Shahani, A. R., and Fariborz, S. J., 1997, "Analysis of an Isotropic Finite Wedge Under Antiplane Deformation," Int. J. Solids Struct., **34**(1), pp. 113–128.
[7] Shahani, A., 1999, "Analysis of an Anisotropic Finite Wedge Under Antiplane Deformation," J. Elast., **34**(I), pp. 17–32.
[8] Shahani, A. R., 2005, "Some Problems in the Antiplane Shear Deformation of Bi-Material Wedges," Int. J. Solids Struct., **42**(11–12), pp. 3093–3113.
[9] Leguillon, D., and Abdelmoula, R., 2000, "Mode III Near and Far Fields for a Crack Lying in or Along a Joint," Int. J. Solids Struct., **37**(19), pp. 2651–2672.

[10] Tuyet, D. T. B., Halpern, L., and Marigo, J.-J., 2018, "Study of the Influence of Small Defects Near a Singular Point in Antiplane Elasticity by an Asymptotic Method," Vietnam J. Mech., **40**(1), pp. 15–32.
[11] Mishuris, G. S., Movchan, N. V., and Movchan, A. B., 2006, "Steady-State Motion of a Mode-III Crack on Imperfect Interfaces," Q. J. Mech. Appl. Math., **59**(4), pp. 487–516.
[12] Paggi, M., and Carpinteri, A., 2008, "On the Stress Singularities at Multimaterial Interfaces and Related Analogies With Fluid Dynamics and Diffusion," ASME Appl. Mech. Rev., **61**(2), p. 20801.
[13] Savruk, M. P., and Kazberuk, A., 2017, *Stress Concentration at Notches*, Springer, New York.
[14] Frishter, L., 2018, "Stress-Deformed State in the Plane Domain Boundary Angle Cutout Zone," Proceedings of the MATEC Web of Conferences, Rostov-on-Don, Russia, Sept. 17–21.
[15] Beom, H. G., and Jang, H. S., 2012, "Analysis of a Wedge in an Anisotropic Bimaterial Under Antiplane Loads," Int. J. Precis. Eng. Manuf., **13**(4), pp. 547–555.
[16] Eder, M. A., and Sarhadi, A., 2020, "A Semi-Analytical Stress Correction Method for Bi-Material Mode-III V-Notches," Theor. Appl. Fract. Mech., **106**, p. 102443.
[17] Jiménez-Alfaro, S., and Mantič, V., 2023, "Crack Tip Solution for Mode III Cracks in Spring Interfaces," Eng. Fract. Mech., **288**, p. 109293.
[18] Bahrami, B., Ayatollahi, M. R., Mehraban, M. R., Nejati, M., and Berto, F., 2022, "On the Effects of Higher Order Stress Terms in Pure Mode III Loading of Bi-Material Notches," Fatigue Fract. Eng. Mater. Struct., **45**(11), pp. 3333–3346.
[19] Mirzaei, A. M., Ayatollahi, M. R., Bahrami, B., and Berto, F., 2021, "A New Unified Asymptotic Stress Field Solution for Blunt and Sharp Notches Subjected to Mixed Mode Loading," Int. J. Mech. Sci., **193**(Oct.), p. 106176.
[20] Mirzaei, A. M., Bahrami, B., and Ayatollahi, M. R., 2022, "Asymptotic Stress Field Around the Blunt and Sharp Notches in Bimaterial Media Under Mixed Mode I/II Loading," Appl. Math. Modell., **109**, pp. 848–863.
[21] Eder, M. A., Bitsche, R. D., Nielsen, M., and Branner, K., 2014, "A Practical Approach to Fracture Analysis at the Trailing Edge of Wind Turbine Rotor Blades," Wind Energy, **17**(3), pp. 483–497.
[22] Mirzaei, A. M., Ayatollahi, M. R., Bahrami, B., and Berto, F., 2020, "Elastic Stress Analysis of Blunt V-Notches Under Mixed Mode Loading by Considering Higher Order Terms," Appl. Math. Modell., **78**, pp. 665–684.
[23] Mirzaei, A. M., Ayatollahi, M. R., and Bahrami, B., 2019, "Asymptotic Stress Field and the Coefficients of Singular and Higher Order Terms for V-Notches With End Holes Under Mixed-Mode Loading," Int. J. Solids Struct., **172–173**, pp. 51–69.
[24] Qian, J., and Hasebe, N., 1997, "Property of Eigenvalues and Eigenfunctions for an Interface V-Notch in Antiplane Elasticity," Eng. Fract. Mech., **56**(6), pp. 729–734.